Inorg. Chem. **2006**, *45*, 8922–8929

Solvent-Enhanced Magnetic Ordering Temperature for Mixed-Valent Chromium Hexacyanovanadate(II), $Cr^{II}_{0.5}Cr^{III}[V^{II}(CN)_6]\cdot z$MeCN, Magnetic Materials

Kendric J. Nelson, Ian D. Giles, Shayla A. Troff, Atta M. Arif, and Joel S. Miller*

Department of Chemistry, University of Utah, 315 South 1400 East Street, Room 2020, Salt Lake City, Utah 84112-0850

Received May 22, 2006

The reaction of $V^{III}(THF)_3Cl_3$ with NEt_4CN in acetonitrile (MeCN) forms $(NEt_4)_3[V^{III}(CN)_6]\cdot 4$MeCN (**1**), which after characterization was used as a molecular building block toward the synthesis of Prussian blue structured magnets. The reaction of **1** with $[Cr^{II}(NCMe)_4](BF_4)_2$ forms $Cr^{II}_{0.5}Cr^{III}[V^{II}(CN)_6]\cdot z$MeCN via internal electron transfer, whose structure and magnetic properties are dependent on the degree of solvation, *z*. When solvated, $Cr^{II}_{0.5}Cr^{III}[V^{II}(CN)_6]\cdot 1.2$MeCN (**2**) is a mixture of crystalline and amorphous fractions that yield a material with two magnetic phases: bulk ferrimagnetic phase/crystalline [faced-centered-cubic lattice with $a = 10.55(2)$ Å] and cluster-glass phase/amorphous. The bulk ferrimagnetic phase exhibits a critical temperature, T_c, of 110 K, while the amorphous cluster-glass phase exhibits a freezing temperature, T_f, of ~25 K. Amorphous $Cr^{II}_{0.5}Cr^{III}[V^{II}(CN)_6]\cdot 0.1$MeCN (**3**) was determined to be the pure cluster-glass phase. This is an overall enhancement of 85 K (350%) in the magnetic ordering temperature via solvation, *z*. The coercivity was also increased 4-fold from 890 (**2**) and 3900 Oe (**3**) via desolvation.

Introduction

Ferrimagnetic, and to a lesser extent ferromagnetic, ordering has been established for several hexacyanometalate-based materials[1−3] possessing the cubic Prussian blue structure.[4] High-critical-temperature, T_c, magnetic materials may find applications in many areas including magnetic shielding[5] and spintronic memory storage devices.[6] Examples of high-T_c Prussian blue structured ferrimagnets include $Cr^{II}_{1.5}[Cr^{III}(CN)_6]\cdot 5H_2O$ ($T_c = 240$ K),[7] $Cr^{III}[Cr^{III}(CN)_6]_{0.93}[Cr^{II}(CN)_6]_{0.05}$ ($T_c = 260$ K),[8] and several vanadium hexacyanochromate room-temperature magnets: $V^{II}_{0.42}V^{III}_{0.58}[Cr^{III}(CN)_6]_{0.86}\cdot 2.8H_2O$ ($T_c = 315$ K),[2a] $V^{II}_{0.45}V^{III}_{0.53}(V^{IV}O)_{0.02}[Cr^{III}CN)_6]_{0.69}(SO_4)_{0.23}\cdot 3.0H_2O\cdot 0.02K_2SO_4$ ($T_c = 310$ K),[2b] and $Cs_{0.82}V^{II}_{0.66}(V^{IV}O)_{0.34}Cr^{III}(CN)_6]_{0.92}(SO_4)_{0.203}\cdot 3.6H_2O$ ($T_c = 315$ K)[2b] reported by Verdaguer and co-workers. Subsequently, $K_{0.50}V^{II}_{0.65}V^{III}_{0.35}[Cr(CN)_6]_{0.95}\cdot 1.7H_2O$ ($T_c = 350$ K),[3a] $KV^{II}[Cr^{III}(CN)_6]\cdot 2H_2O\cdot 0.1KO_3SCF_3$,[3b] and $K_{0.058}V^{II}_{0.57}V^{III}_{0.43}[Cr^{III}(CN)_6]_{0.79}\cdot(SO_4)_{0.058}\cdot 0.93H_2O$[3a] with a similar T_c (~100 °C) were reported.

* To whom correspondence should be addressed. Email: jsmiller@chem.utah.edu.

(1) Verdaguer, M.; Girolami, G. S. In *Magnetism—Molecules to Materials*; Miller, J. S., Drillon, M., Eds.; Wiley-VCH: Weinheim, Germany, 2005; Vol. 5, pp 283−346.

(2) (a) Ferlay, S.; Mallah, T.; Ouahes, R.; Veillet, P.; Verdaguer, M. *Nature* **1995**, *378*, 701. (b) Dujardin, E.; Ferlay, S.; Phan, X.; Desplanches, C.; Moulin, C. C. D.; Sainctavit, P.; Baudelet, F.; Dartyge, E.; Veillet, P.; Verdaguer, M. *J. Am. Chem. Soc.* **1998**, *120*, 11347. (c) Ferlay, S.; Mallah, T.; Ouahes, R.; Veillet, P.; Verdaguer, M. *Inorg. Chem.* **1999**, *38*, 229. (d) Verdaguer, M.; Bleuzen, A.; Marvaud, V.; Vaissermann, J.; Seuleiman, M.; Desplanches, C.; Scuiller, A.; Train, C.; Garde, R.; Gelly, G.; Lomenech, C.; Rosenman, I.; Veillet, P.; Cartier, C.; Villain, F. *Coord. Chem. Rev.* **1999**, *190−192*, 1023. (e) Verdaguer, M.; Bleuzen, A.; Train, C.; Garde, R.; Fabrizi de Biani, F.; Desplanches, C. *Philos. Trans. R. Soc. London A* **1999**, *357*, 2959. (f) Hashimoto, K.; Ohkoshi, S. *Philos. Trans. R. Soc. London A* **1999**, *357*, 2977.

(3) (a) Hatlevik, Ø.; Buschmann, W. E.; Zhang, J.; Manson, J. L.; Miller, J. S. *Adv. Mater.* **1999**, *11*, 914. (b) Holmes, S. M.; Girolami, G. S. *J. Am. Chem. Soc.* **1999**, *121*, 5593.

(4) Ludi, A.; Güdel, H. U. *Struct. Bonding* **1973**, *14*, 1.

(5) (a) Morin, B. G.; Hahm, C.; Epstein, A. J.; Miller, J. S. *J. Appl. Phys.* **1994**, *75*, 5782. (b) Miller, J. S. *Adv. Mater.* **1994**, *6*, 322. (c) Landee, C. P.; Melville, D.; Miller, J. S. In *NATO ARW Molecular Magnetic Materials*; Kahn, O., Gatteschi, D., Miller, J. S., Palacio, F., Eds.; Kluwer Academic Publishers: London, 1991; Vol. E198, p 395.

(6) Prigodin, V. N.; Raju, N. P.; Pokhodnya, K. I.; Miller, J. S.; Epstein, A. J. *Adv. Mater.* **2002**, *14*, 1230.

(7) Mallah, T.; Thiébaut, S.; Verdaguer, M.; Veillet, P. *Science* **1993**, *262*, 1554.

(8) (a) Buschmann, W. E.; Paulson, S. C.; Wynn, C. M.; Girtu, M.; Epstein, A. J.; White, H. S.; Miller, J. S. *Adv. Mater.* **1997**, *9*, 645. (b) Buschmann, W. E.; Paulson, S. C.; Wynn, C. M.; Girtu, M.; Epstein, A. J.; White, H. S.; Miller, J. S. *Chem. Mater.* **1998**, *10*, 1386.

10.1021/ic0608896 CCC: $33.50
Published on Web 10/03/2006

Because of the high T_c's observed for the vanadium hexacyanochromate family of magnets, we sought to prepare chromium hexacyanovanadate analogues and compare their magnetic behaviors. $K_4[V^{III}(CN)_7]\cdot 2H_2O$[9] has been prepared; however, it is hydrolytically unstable without excess CN in solution.[9e] Therefore, a nonaqueous soluble cyanovanadate(III) was sought, and $(NEt_4)_4[V^{III}(CN)_7]$ was targeted for synthesis. Albeit seven-coordinate and may not form the ideal Prussian blue structure, many heptacyanomolybdate(III)-based magnets have been reported.[10] Along with enhancing T_c, external stimulations that modulate the magnetic behavior are of interest in the areas of molecular switches[11] and/or sensors.[12] Photoinduced,[13] pressure-induced,[14] and electrochemically induced[15] changes in magnetic properties have been observed, and recently the T_c of $K_{0.2}Mn_{1.4}[Cr(CN)_6]\cdot 6H_2O$ could be reversibly increased from 66 to 99 K upon dehydration.[12] Herein, we report the formation of $(NEt_4)_3[V^{III}(CN)_6]$ (**1a**), not the expected $[V^{III}(CN)_7]^{4-}$, and magnets based on the its reaction with $[Cr^{II}(NCMe)_6]^{2+}$.

Experimental Section

All manipulations were carried out under a dry N_2 atmosphere (<1 ppm O_2) using Schlenck techniques or in a Vacuum Atmospheres DriLab. $V^{III}Cl_3(THF)_3$,[16] $[Cr^{II}(NCMe)_4](BF_4)_2$,[17] and NEt_4CN[18] were prepared via literature routes. Acetonitrile (MeCN) was purified through an activated alumina dual column purification system under a positive pressure of N_2, while diethyl ether (Et_2O) was purified via distillation under a positive dry N_2 pressure using sodium dispersion and benzophenone.

$(NEt_4)_3[V^{III}(CN)_6]\cdot z$MeCN, 1 ($z = 4$) and 1a ($z = 0$). **1** was synthesized by adding a 20-mL MeCN solution of $V^{III}Cl_3(THF)_3$ (454.5 mg, 1.216 mmol, 1 equiv) dropwise to a stirring 250-mL MeCN solution of NEt_4CN (1265.5 mg, 8.098 mmol, 6.7 equiv), resulting in a murky brown solution, which turned green-yellow over approximately 3−4 h, after which the solution was filtered and the filtrate was concentrated to approximately 20 mL under reduced pressure. Green-yellow X-ray-quality crystals were obtained by cooling the solution at −20 °C for 24 h (yield: 612.1 mg, 84%) and characterized by single-crystal X-ray diffraction. The crystallographic sample was maintained in contact with the mother liquor to prevent solvent loss. Thermogravimetric analysis (TGA) and differential scanning calorimetry (DSC) studies showed that the sample was stable up to 175 °C and could be desolvated at room temperature with a constant flow of N_2 over the sample to form the desolvated **1a**. Anal. Calcd for $C_{30}H_{60}N_9V$, **1a**: C, 60.26; H, 10.10; N, 21.18; V, 8.46. Found: C, 59.91; H, 10.46; N, 20.82; V, 7.98. Selected IR data (KBr): ν_{CN} (cm^{-1}) 2107 (m), 2094 (sh), 2066 (w).

$Cr_{1.5}[V(CN)_6]\cdot z$MeCN, 2 ($z = 1.2$) and 3 ($z = 0.1$). **2** and **3** were synthesized by slowly adding a 20-mL MeCN solution of **1a** (300.2 mg, 0.5022 mmol, 2 equiv) via a syringe pump at 10 mL/h into a stirring 20-mL MeCN solution of $[Cr^{II}(NCMe)_4](BF_4)_2$ (293.6 mg, 0.7532 mmol, 3 equiv), resulting in the immediate dark-blue precipitate. After complete addition of the Cr^{II} solution, the mixture was stirred for approximately 30 min. The dark-blue product was collected via centrifugation, the colorless supernate was decanted off, and the product was washed with MeCN (3 × 15 mL), followed by 15 mL of Et_2O. **2** was obtained by drying at room temperature under vacuum for 30 min, while **3** was obtained by drying for a total of 24 h. The elemental analyses of **2** proved inconclusive because of facile solvent loss at room temperature. This was confirmed by TGA coupled with mass spectrometry (TGA/MS), which showed a rapid loss of MeCN at room temperature followed by a continuous gradual mass loss up to 600 °C that was attributed to solvent loss and decomposition (total mass loss of 57.3%). Because of this gradual mass loss, the temperatures at which solvent loss and decomposition occur were not able to be determined. In contrast, elemental analyses of **3** revealed the $Cr_{1.5}[V(CN)_6]\cdot 0.1$MeCN composition: Anal. Calcd for $C_{6.2}H_{0.3}Cr_{1.5}N_{6.1}V$: C, 25.75; H, 0.10; N, 29.55; Cr, 26.97; V, 17.62. Found: C, 25.27; H, 0.90; N, 28.82; Cr, 26.75; V, 17.09. The TGA/MS of **3** showed a gradual mass loss of 43.7% up to 600 °C attributed to solvent loss and decomposition. Again, because of this gradual mass loss, the temperatures at which solvent loss and decomposition occur were not able to be determined. From the difference in mass losses between **2** and **3**, the solvent content of **2** was determined to be $z = 1.2$; hence, **2** is formulated as $Cr_{1.5}[V(CN)_6]\cdot 1.2$MeCN. Both **2** and **3** were stored at −25 °C and immediately studied to avoid a change in the solvent composition, especially for **2**.

X-ray Crystallography. A green prism-shaped crystal of 0.35 × 0.35 × 0.25 mm in size was mounted on a glass fiber with traces of viscous oil and then transferred to a Nonius Kappa CCD diffractometer equipped with Mo Kα radiation. A total of 10 frames of data were collected at 150(1) K with an oscillation range of 1°/frame and an exposure time of 20 s/frame.[19] Indexing and unit cell refinement based on all observed reflections from those 10 frames indicated a monoclinic *C* lattice. A total of 9022 reflections ($\lambda_{max} = 27.49°$) were indexed, integrated, and corrected for Lorentz, polarization, and absorption effects using DENZO-SMN and

(9) (a) Bennett, B. G.; Nicholls, D. *J. Chem. Soc. A* **1971**, 1204. (b) Nast, R.; Rehder, D. *Chem. Ber.* **1971**, *104*, 1709. (c) Towns, R. L. R.; Levenson, R. A. *J. Am. Chem. Soc.* **1972**, *94*, 4345. (d) Levenson, R. A.; Towns, R. L. R. *Inorg. Chem.* **1974**, *13*, 105. (e) Levenson, R. A.; Dominguez, R. J. G.; Willis, M. A.; Young, F. R., III. *Inorg. Chem.* **1974**, *13*, 2761.

(10) For example, see: Larionova, J.; Sanchiz, J.; Gohlen, S.; Ouahab, L.; Kahn, O. *Chem. Commun.* **1998**, 953. Larionova, J.; Clérac, R.; Sanchiz, J.; Kahn, O.; Golhen, S.; Ouahab, L. *J. Am. Chem. Soc.* **1998**, *120*, 13088. Kahn, O.; Larionova, J.; Ouahab, L. *Chem. Commun.* **1999**, 945. Rombaut, G.; Golhen, S.; Ouahab, L.; Mathonière, C.; Kahn, O. *J. Chem. Soc., Dalton Trans.* **2000**, 3609. Larionova, J.; Clérac, R.; Donnadieu, B.; Guérin, C. *Chem.—Eur. J.* **2002**, *8*, 2712. Tanase, S.; Tuna, F.; Guionneau, P.; Maris, T.; Rombaut, G.; Mathonière, C.; Andruh, M.; Kahn, O.; Sutter, J.-P. *Inorg. Chem.* **2003**, *42*, 1625. Le Goff, X. F.; Willemin, S.; Coulon, C.; Larionova, J.; Donnadieu, B.; Clérac, R. *Inorg. Chem.* **2004**, *43*, 4784.

(11) Sato, O. *Acc. Chem. Res.* **2003**, *36*, 692. Sato, O.; Kawakami, T.; Kimura, M.; Hishiya, S.; Kubo, S.; Yasuaki, E. *J. Am. Chem. Soc.* **2004**, *126*, 13176. Sato, O. *J. Photochem. Photobiol., C: Photochem. Rev.* **2004**, *5*, 203. Verdaguer, M.; Villain, F.; Ouahès, R.; Galvez, N.; Garde, R.; Keller, G.; Tournilhac, F. *Polyhedron* **2005**, *24*, 2906.

(12) Lü, Z.; Wang, X.; Liu, Z.; Liao, F.; Gao, S.; Xiong, R.; Ma, H.; Zhang, D.; Zhu, D. *Inorg. Chem.* **2006**, *45*, 999.

(13) Sato, O.; Iyoda, T.; Fujishima, A.; Hashimoto, K. *Science* **1996**, *272*, 704.

(14) Sato, O.; Einga, Y.; Fujishima, A.; Hashimoto, K. *Inorg. Chem.* **1999**, *38*, 4405. Bleuzen, A.; Lomenech, C.; Escax, V.; Villain, F.; Varret, F.; Moulin, C. C. D.; Verdaguer, M. *J. Am. Chem. Soc.* **2000**, *122*, 6648. Coronado, E.; Giménez-López, M. C.; Levchenko, G.; Romero, F. M.; Garcia-Baonza, V.; Milner, A.; Paz-Pasternak, M. *J. Am. Chem. Soc.* **2005**, *127*, 4850.

(15) Sato, O.; Iyoda, T.; Fujishima, A.; Hashimoto, K. *Science* **1996**, *271*, 49.

(16) Gansauer, A.; Rinker, B. *Tetrahedron* **2002**, *58*, 7017.

(17) (a) Henriques, R. T.; Herdtweck, E.; Kühn, F. E.; Lopes, A. D.; Mink, J.; Ramão, C. C. *J. Chem. Soc., Dalton Trans.* **1998**, 1293. (b) Buschmann, W. E.; Arif, A. M.; Miller, J. S. *Chem.—Eur. J.* **1998**, *4*, 1731.

(18) Andreades, S.; Zahnow, E. W. *J. Am. Chem. Soc.* **1969**, *91*, 4181.

(19) *COLLECT Data Collection Software*; Nonius BV: Delft, The Netherlands, 1998.

Table 1. Crystallographic Data for **1**

empirical formula	$C_{38}H_{72}N_{13}V$
fw, g mol^{-1}	762.03
T, K	150(1)
space group	*C*2/*c*
a, Å	27.0991(14)
b, Å	12.2152(6)
c, Å	18.0266(8)
α, deg	90
β, deg	130.270(2)
γ, deg	90
Z	4
V, Å^3	4553.0(4)
density (calcd), Mg m^{-3}	1.112
abs coeff, μ, mm^{-1}	0.258
R1(*F*)[a]	0.0736
wR2(F^2)[a]	0.1867
S	1.028
wavelength, Å	0.71073

[a] $R1 = \sum(||F_o| - |F_c||)/\sum|F_o|$, $wR2 = [\sum w(F_o^2 - F_c^2)^2)/\sum(F_o^2)^2]^{1/2}$, and S = goodness of fit on $F^2 = [\sum(w(F_o^2 - F_c^2)^2/(n - p)]^{1/2}$, where n is the number of reflections and p is the number of parameters refined.

SCALEPAC.[20] The structure was solved by a combination of direct methods and heavy atoms using *SIR97*.[21] All of the non-H atoms were refined with anisotropic displacement coefficients. H atoms were assigned isotropic displacement coefficients $U(H) = 1.2U(C)$ or $1.5U(C_{methyl})$, and their coordinates were allowed to ride on their respective C atoms using *SHELXL97*.[22] The V atom is sitting on the inversion center, and one of the tetraethylammonium cations exhibits orientation disorder due to sitting on the 2-fold axis. The weighting scheme employed was $w = 1/[\sigma^2(F_o^2) + (0.1035P)^2 + 5.9048P]$ where $P = (F_o^2 + 2F_c^2)/3$. The maximum Δ/σ in the final cycle of the least squares was 0, and the residual peaks on the final difference Fourier map ranged from -0.355 to $+0.833$ e/Å^3. Scattering factors were taken from the *International Tables for Crystallography*, Vol. C.[23] Crystal data for **1** is summarized in Table 1.

Physical Methods. IR spectra (KBr) were recorded from 400 to 4000 cm^{-1} on a Bruker Tensor 37, and a variable-temperature Specac cryostat was used for temperature-dependent studies. Electronic absorption spectra were recorded from 10 000 to 50 000 cm^{-1} on an Ocean Optics HR2000 spectrophotometer equipped with fiber-optic cables fed through the wall of a Vacuum Atmospheres DriLab under an inert atmosphere and were taken in 1.0-cm quartz cells.

TGA/MS measurements were studied on a TA Instruments model 2050 TGA analyzer coupled to a Thermolab TL1285 thermal analysis/mass spectrometer. The TGA operates between ambient temperature and 1000 °C and is located in a Vacuum Atmospheres DriLab under an inert atmosphere. TGA samples were handled in a N_2 atmosphere and heated under a N_2 purge. Heating rates were 5 °C/min. DSC was measured on a TA Instruments model 2910 DSC with heating rates of 3 °C/min. DSC samples were weighed and hermetically sealed in Al pans under a N_2 gas atmosphere. Elemental analyses were performed by GCL & Chemisar Laboratories (Guelph, Ontario, Canada).

Powder X-ray diffraction (XRD) scans were obtained on a $\theta-\theta$ Bruker AXS D8 Advance diffractometer (2θ of 5−85°, step width of 0.02°, counting time of 10 s/step, voltage of 40 kV, and current of 40 mA) fitted with a Göbel mirror to remove all but the Cu Kα radiation (λ = 1.540 60 Å). Samples were sealed under an inert atmosphere in 1.00-mm thin-walled quartz capillaries to prevent oxidation, and scans were performed at room temperature (~298 K).

Magnetic susceptibility measurements were made between 5 and 300 K using a Quantum Design MPMS-5 5T SQUID magnetometer with a sensitivity of 10^{-8} or 10^{-12} emu/Oe at 1 T and equipped with an ultralow-field (~0.005 Oe), reciprocating sample measurement system, and continuous low-temperature control with enhanced thermometry features, or using a Quantum Design PPMS-9 ac/dc susceptometer. Measurements were made on powders contained in airtight Delrin holders supplied by Quantum Design. Small amounts of quartz wool were used in the Delrin holders to minimize the movement of the powders during measurements, and minimal amounts of heavy Nujol (Aldrich) was used to aid in protecting the sample from solvent loss and exposure to air. Because of the extreme sensitivity of some samples to solvent loss and all to oxidation, the samples were stored at −20 °C in a Vacuum Atmospheres DriLab. Samples were loaded immediately after removal from the freezer. The data were corrected for the measured diamagnetism of each holder and Nujol. Core diamagnetic corrections of -394, -145, and -114×10^{-6} emu/mol were calculated from standard diamagnetic susceptibility tables for **1a**, **2**, and **3**, respectively.

Results and Discussion

$(NEt_4)_3[V^{III}(CN)_6]\cdot zMeCN$, 1 ($z$ = 4) and 1a (z = 0). The reaction of $V^{III}Cl_3(THF)_3$ and NEt_4CN in MeCN led to a green-yellow solution, from which X-ray-quality crystals were obtained by slowly cooling to −25 °C. Single-crystal X-ray analysis revealed that unexpectedly **1** formed. **1** could be desolvated at room temperature under a constant flow of N_2 to form **1a**, and TGA and DSC showed that **1a** was stable up to 175 °C (Figure S1 in the Supporting Information) by the start of the mass loss in the TGA data at ~175 °C and the lack of any heat flow transition in DSC. **1** is isostructural with $(NEt_4)_3[Cr^{III}(CN)_6]\cdot 4MeCN$[24a] and $(NEt_4)_3[Ti^{III}(CN)_6]\cdot 4MeCN$[24b] (Figure 1). The 2.087(3)-Å V−C2 distance is shorter than the V−C1 [2.140(3) Å] and V−C3 [2.155(3) Å] distances, indicative of a tetragonal compression arising from a Jahn−Teller distortion expected for a V^{III} d^2 octahedral complex with a triply degenerate ground state ($^3T_{1g}$).[25] The average V−C distance of 2.127(3) Å is slightly shorter than that observed for $K_4[V^{III}(CN)_7]\cdot 2H_2O$ [average = 2.147(7) Å].[9c,d] **1a** exhibits a strong sharp ν_{CN} absorption at

(20) Otwinowski, Z.; Minor, W. *Methods Enzymol.* **1997**, *276*, 307.

(21) Altomare, A.; Burla, M. C.; Camalli, M.; Cascarano, G.; Giacovazzo, C.; Guagliardi, A.; Moliteni, A. G. G.; Polidori, G.; Spagna, R. *SIR97—A program for automatic solution and refinement of crystal structure*, Release 1.02; University of Göttingen: Göttingen, Germany, 1997.

(22) Sheldrick, G. M. *SHELX97* [includes *SHELXS97*, *SHELXL97*, and *CIFTAB*] *Programs for Crystal Structure Analysis*, Release 97-2; University of Göttingen: Göttingen, Germany, 1997.

(23) (a) Maslen, E. N.; Fox, A. G.; O'Keefe, M. A. In *International Tables for Crystallography: Mathemetical, Physical and Chemical Tables*; Wilson, A. J. C., Ed.; Kluwer: Dordrecht, The Netherlands, 1992; Vol. C, Chapter 6, pp 476−516. (b) Creagh, D. C.; McdAuley, W. J. *International Tables for Crystallography: Mathematical, Physical and Chemical Tables*; Wilson, A. J. C., Ed.; Kluwer: Dordrecht, The Netherlands, 1992; Vol. C, Chapter 4, pp 206−222.

(24) (a) Nelson, K. J.; Arif, A. M.; Miller, J. S., unpublished results. (b) Entley, W. R.; Treadway, C. R.; Wilson, S. R.; Girolami, G. S. *J. Am. Chem. Soc.* **1997**, *119*, 6251. Here $(NEt_4)_3[Ti^{III}(CN)_6]\cdot 4MeCN$ is reported to have the *I*2/*a* space group. *I*2/*a* and *C*2/*c* are crystallographically equivalent via a (0 0 1, 0 1 0, −1 0 −1) transformation. Therefore, **1** and $(NEt_4)_3[Ti^{III}(CN)_6]\cdot 4MeCN$ are isostructural.

(25) Huheey, J. E.; Keiter, E. A.; Keiter, R. L. *Inorganic Chemistry: Principles of Structure and Reactivity*, 4th ed.; Harper Collins College Publishers: New York, 1993; pp 449−450.

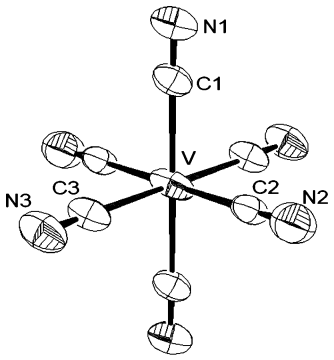

Figure 1. ORTEP atom labeling diagram of **1** (50% probability level; cations and solvent molecules are omitted for clarity) with V−C1 = 2.140(3) Å, V−C2 = 2.087(3) Å, and V−C3 = 2.155 (3) Å.

2107 cm^{-1} and a weak broad ν_{CN} absorption at 2066 cm^{-1} [half-width at half-height (hwhh): 4.4 and 12.1 cm^{-1}, respectively; Figure S2 in the Supporting Information]. These are comparable to the ν_{CN} absorptions at 2100 (s) and 2070 (m) cm^{-1} observed for $K_4[V^{III}(CN)_7]\cdot 2H_2O$.[9e] The MeCN-solution UV−vis spectrum of $[V^{III}(CN)_6]^{3-}$ has absorptions at 15 950 cm^{-1} ($\lambda = 627$ nm, $\epsilon = 4$ M^{-1} cm^{-1}), 22 960 cm^{-1} (436 nm, 23 M^{-1} cm^{-1}), 31 920 cm^{-1} (313 nm, 1570 M^{-1} cm^{-1}), and 40 180 cm^{-1} (249 nm, 3903 M^{-1} cm^{-1}) (Figure S3 in the Supporting Information) and differs from $K_4[V^{III}(CN)_7]\cdot 2H_2O$ with absorptions observed at 22 200 cm^{-1} ($\lambda = 450$ nm, $\epsilon = 36$ M^{-1} cm^{-1}), 28 300 cm^{-1} (353 nm, 57 M^{-1} cm^{-1}), and 40 000 cm^{-1} (250 nm, 2000 M^{-1} cm^{-1}).[9a]

The 5−300 K magnetic susceptibility, χ, of **1a** has a room-temperature χT value of 0.778 emu K mol^{-1} [corrected for temperature-independent paramagnetism (TIP); Figure 2]. This is reduced from the 1.00 emu K mol^{-1} spin-only value, which is attributed to $g < 2$ and antiferromagnetic coupling. Above 50 K, $\chi(T)$ could be fit to the Curie−Weiss expression, $\chi \propto (T - \theta)^{-1}$, with $g = 1.82$, $\theta = -26$ K, and TIP = 50×10^{-6} emu mol^{-1}. These values are in good agreement with $g = 1.88$ reported for $K_3[V^{III}(NCS)_6]\cdot 4H_2O$, $-31 < \theta < -1$ K, and a TIP in the range of $75 \pm 25 \times 10^{-6}$ emu mol^{-1} for V^{III} complexes.[26]

$Cr_{1.5}[V(CN)_6]\cdot$zMeCN, 2 ($z = 1.2$) and 3 ($z = 0.1$). The reaction of **1a** with $[Cr^{II}(NCMe)_4](BF_4)_2$ in MeCN led to the formation of a dark-blue precipitate of formulation $Cr_{1.5}[V(CN)_6]\cdot$zMeCN, whose structure and magnetic properties depend significantly on the degree of solvation, *z*. Both the solvated (**2**) and desolvated (**3**) compounds exhibit ν_{CN} absorptions at 2093 (s/br) cm^{-1} [hwhh = 24.5 and 23.7 cm^{-1}, respectively (Figure S2 in the Supporting Information)[27]], suggesting that their structures are independent of *z*. The value of *z* in a dried sample was determined by elemental analysis to be 0.1, while the composition of the solvated product, which proved difficult to obtain from elemental analyses, because of facile solvent loss at room temperature, was determined from TGA/MS studies prior to drying to be $Cr_{1.5}[V(CN)_6]\cdot 1.2$MeCN (**2**).

These ν_{CN} absorptions are shifted to lower energy with respect to $[V^{III}(CN)_6]^{3-}$ (2107 cm^{-1}). This is opposite to the dominant trend of ν_{CN} shifting to higher energy upon bridging to another metal as a consequence of depopulation of the electron density from the 5σ orbital.[28] In contrast, this trend is not observed for the high-T_c vanadium hexacyanochromate family of magnets where ν_{CN} decreases to 2111 ± 7 cm^{-1} [2,3] from 2132 cm^{-1} for $K_3[Cr^{III}(CN)_6]$[3a] and there is little to no shift from 2111 cm^{-1} for $(NEt_4)_3[Cr^{III}(CN)_6]$.[24] This decrease in the ν_{CN} frequency is attributed to enhanced π-back-bonding to V with respect to Cr and, to our knowledge, has not been reported for other systems.[3a] Thus, because of the observed ν_{CN} 14 cm^{-1} decrease with respect to $[V^{III}(CN)_6]^{3-}$, the assignment of the oxidation states is not straightforward.[29] On the basis of the $Cr_{1.5}[V(CN)_6]\cdot$zMeCN composition and charge neutrality, formulations (i) $Cr^{II}_{1.5}[V^{III}(CN)_6]\cdot$zMeCN, (ii) $Cr^{II}_{0.5}Cr^{III}[V^{II}(CN)_6]\cdot$zMeCN, and (iii) $Cr^{II}_{0.5}V^{II}[Cr^{III}(CN)_6]\cdot$zMeCN are reasonable for **2** and **3**.

For formulation i, ν_{CN} should shift to higher frequency, as is typically observed; however, because of the observed 14-cm^{-1} decrease in the frequency, this formulation is unlikely. Formulations ii and iii are identical with respect to oxidation states, composition, and magnetic properties, except the CN is C-bound to a different metal ion in each of the formulations. Both formulations ii and iii require an electron transfer from Cr^{II} to V^{III}, resulting in Cr^{III} and V^{II}, respectively. This type of electron transfer has been seen between Fe^{II} and Fe^{III} in Turnbull's blue.[30] For formulation ii, $[V^{III}(CN)_6]^{3-}$ would be reduced to $[V^{II}(CN)_6]^{4-}$ in the solid state, yielding $V^{II}-CN-Cr^{III}$ linkages. The observed 2093-cm^{-1} absorption is consistent with this linkage because it is higher in energy than the 2065-cm^{-1} absorption observed for $K_4[V^{II}(CN)_6]$.[9b] Furthermore, it is similar to the 2097-cm^{-1} absorption reported for $Cs_2Mn^{II}[V^{II}(CN)_6]$,[31] which has this $V^{II}-CN-M$ linkage.

Formulation iii, in addition to the same electron transfer, requires a linkage isomerization, i.e., $V^{II}-CN-Cr^{III} \rightarrow V^{II}-NC-Cr^{III}$. Several examples of Prussian blue structures exhibiting linkage isomerization have been reported to occur in the solid state.[14c,32] Formulation iii is similar to electrochemically prepared $K_aV^{II/III}_xCr^{II}_{1-x}[Cr^{III}(CN)_6]\cdot zH_2O$,[33] where for $0.46 \le x \le 0.55$ two ν_{CN} absorptions at 2166 and 2112 cm^{-1} corresponding to $Cr^{III}-CN-Cr^{II}$ and $Cr^{III}-CN-V^{II/III}$ linkages, respectively, are observed. Hence, this pair of ν_{CN} absorptions is expected for **2** and **3**, and because of their absence, formulation iii is also unlikely.

(26) Boudreaux, E. A.; Mulay, L. N. *Theory and Applications of Molecular Paramagnetism*; Wiley-Interscience: New York, 1976; p 159. Figgis, B. N.; Lewis, J.; Mabbs, F. *J. Chem. Soc.* **1960**, 2480.
(27) Exposure to air results in oxidation, leading to the growth of absorptions at ~2160 and ~983 cm^{-1} indicative of vanadyl formation.
(28) Nakamoto, K. *Infrared and Raman Spectra of Inorganic and Coordination Compounds Part B: Applications in Coordination, Organometallic, and Bioinorganic Chemistry*, 5th ed.; Wiley-Interscience: New York, 1997; p 111.
(29) X-ray photoelectron spectroscopy proved inconclusive as a result of the high air sensitivity of the products.
(30) For example, see: Muller, E. *J. Prakt. Chem.* **1912**, *84*, 353. Maer, K., Jr.; Beasley, M. L.; Collins, R. L.; Milligan, W. O. *J. Am. Chem. Soc.* **1968**, *90*, 3201. Cosgrove, J. G.; Collins, R. L.; Murty, D. S. *J. Am. Chem. Soc.* **1973**, *95*, 1083.
(31) Entley, W. R.; Girolami, G. S. *Science* **1995**, *268*, 397.
(32) For example, see: Brown, D. B.; Shriver, D. F.; Anderson, S. E. *Inorg. Chem.* **1965**, *4*, 725. Entley, W. R.; Girolami, G. S. *Inorg. Chem.* **1994**, *33*, 5165. Buschmann, W. E.; Ensling, J.; Gütlich, P.; Miller, J. S. *Chem.—Eur. J.* **1999**, *5*, 3019.
(33) Mizuno, M.; Ohkoshi, S.; Hashimoto, K. *Adv. Mater.* **2000**, *12*, 1955.

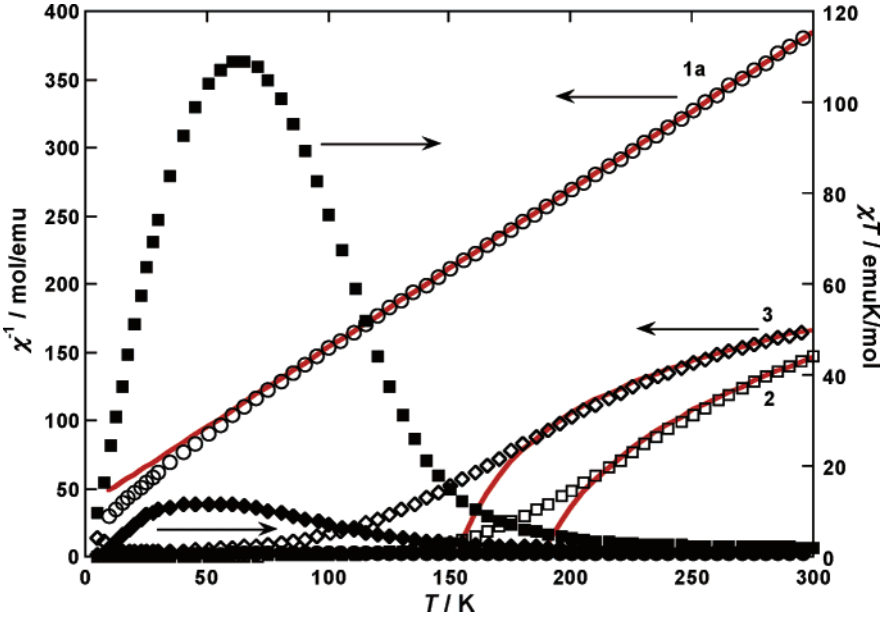

Figure 2. $\chi T(T)$ (filled symbols) and $\chi^{-1}(T)$ (open symbols) of **1a** (○, ●), $Cr^{II}_{0.5}Cr^{III}[V^{II}(CN)_6]\cdot 1.2MeCN$ (**2**) (■, □), and $Cr^{II}_{0.5}Cr^{III}[V^{II}(CN)_6]\cdot 0.1MeCN$ (**3**) (◇, ◆) at 500 Oe. Fits to $\chi^{-1}(T)$ using the Curie−Weiss law for **1a** (○, ●) and Néel's hyperbolic equation for $Cr^{II}_{0.5}Cr^{III}[V^{II}(CN)_6]\cdot 1.2MeCN$ (**2**) (■, □) and $Cr^{II}_{0.5}Cr^{III}[V^{II}(CN)_6]\cdot 0.1MeCN$ (**3**) (◇, ◆) are displayed with solid lines.

Formulation ii might be thermally transformed into formulation iii; thus, the temperature-dependent IR spectra were monitored (Figure S4 in the Supporting Information). Upon heating to 90 °C, the broad 2093-cm^{-1} absorption present for both **2** and **3** shifts to 2099 cm^{-1} and a shoulder at ∼2160 cm^{-1} appears. Upon heating to 130 °C, the absorption shifts to 2105 cm^{-1} and the shoulder becomes more pronounced at ∼2150 cm^{-1}. This shift and shoulder growth continues up to 250 °C, where heating was stopped to avoid decomposition. At 250 °C, the ν_{CN} absorption had shifted to 2109 cm^{-1} and the shoulder grew into a clear absorption at 2152 cm^{-1}. The sample was then held at 200 °C for 36 h, which resulted in a small change, with the main ν_{CN} absorption now at 2110 cm^{-1} and the shoulder that grew into the absorption shifted to 2156 cm^{-1}. This shift of 17 cm^{-1} from 2093 to 2110 cm^{-1} is attributed to the aforementioned linkage isomerization of $V^{II}-CN-Cr^{III}$ to $V^{II}-NC-Cr^{III}$, and the 2156-cm^{-1} shoulder that became an absorption at higher temperature is also consistent with this linkage isomerization to form $Cr^{II}-NC-Cr^{III}$ linkages. Hence, **2** and **3** are respectively formulated as $Cr^{II}_{0.5}Cr^{III}[V^{II}(CN)_6]\cdot zMeCN$ ($z = 1.2$ and 0.1).

The powder XRD pattern of **2** (Figure S5a in the Supporting Information) was indexed to a face-centered-cubic (fcc) structure, $a = 10.55(2)$ Å, similar to Prussian blue and its analogues;[4] however, the presence of broad peaks suggests a significant amount of amorphous material. In contrast, the diffraction pattern of **3** had weak, broad peaks indicative of the material being completely amorphous and could not be indexed to a fcc structure (Figure S5b in the Supporting Information). Consequently, **2** has crystalline and amorphous portions and is structurally more ordered than the almost completely amorphous **3**.

2 and **3** have room-temperature χT values of 2.075 and 1.809 emu K mol^{-1}, respectively. These values are considerably less than the expected spin-only χT value of 5.25 emu K mol^{-1} (for $S = 2$ high-spin Cr^{II}; $S = {}^3/_2$ Cr^{III} and V^{II}) for $Cr^{II}_{0.5}Cr^{III}[V^{II}(CN)_6]\cdot zMeCN$ and are attributed to strong antiferromagnetic coupling between the V^{II} and $Cr^{II/III}$ ions. These χT values require $\theta \sim -460$ and -570 K for **2** and **3**, respectively, and similar values, consistent with strong antiferromagnetic coupling, have been observed.[7,31,34] These large values of θ were confirmed for **3** because θ obtained from $\chi^{-1}(T)$ (360 K $< T \leq$ 400 K) data is -423 K (Figure S6 in the Supporting Information).[35]

The $\chi T(T)$ data reveal large changes in the magnetic properties of **2** and **3** as a function *z*. Ferrimagnetic ordering is anticipated from the gradual increase in $\chi T(T)$ for **2** as the temperature decreases below 275 and increases even more rapidly below 175 K, reaching a maximum of 109 emu K mol^{-1} at 65 K. In contrast, for **3** the χT gradually increases below 225 K with decreasing temperature and increases more rapidly below 150 K, reaching a maximum of ∼12 emu K mol^{-1} at 50 K (Figure 2). $\chi^{-1}(T)$ in the high-temperature region were fit (210−300 and 175−400 K for **2** and **3**, respectively) to the hyperbolic equation based on Néel's theory[36] (Figure 2), and the Néel ordering temperatures, T_N, of 188 and 153 K were deduced for **2** and **3**, respectively. θ values of -150 and -445 K for **2** and **3**, respectively, were obtained from these fits and confirm strong antiferromagnetic coupling in the high-temperature region. These high values of T_N must be taken with caution because the T_N values are dependent on the lower limit of the fitted data. This is due to the unusual nonhyperbolic shape of the $\chi^{-1}(T)$ data, which is likely caused by the multiphase nature of these materials.

(34) Holmes, S. M.; Girolami, G. S. *Mol. Cryst. Liq. Cryst.* **1997**, *305*, 279.
(35) $\chi(T)$ studies above 300 K for **2** were not performed because of solvent loss even at room temperature.
(36) Néel, L. *Ann. Phys.* **1948**, *3*, 137. Smart, J. S. *Am. J. Phys.* **1955**, *23*, 356.

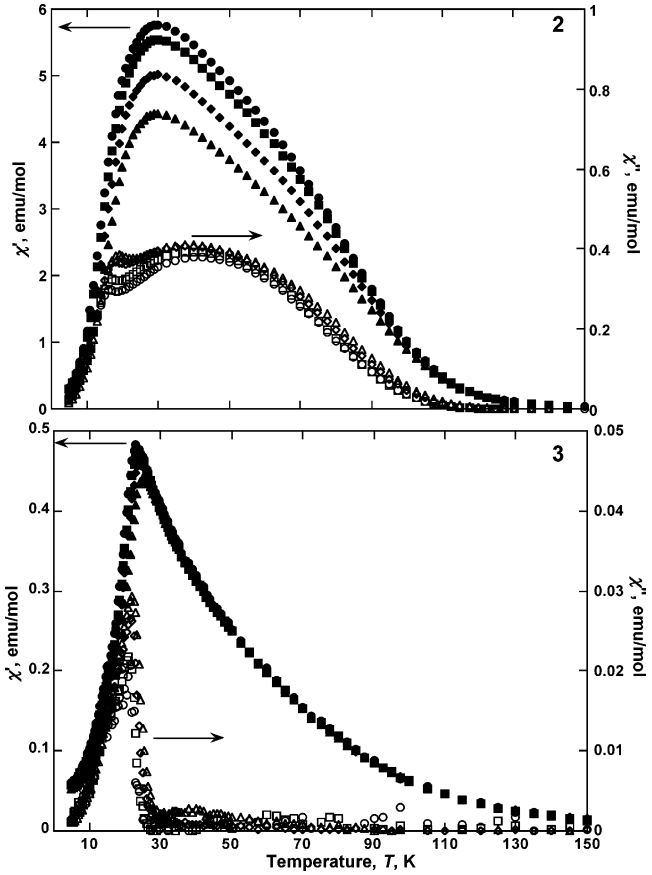

Figure 3. Observed in-phase, $\chi'(T)$ (closed symbols), and out-of-phase, $\chi''(T)$ (open symbols), ac responses for $Cr^{II}_{0.5}Cr^{III}[V^{II}(CN)_6]\cdot 1.2MeCN$ (**2**) (top) at 33 (○, ●), 100 (■, □), 1000 (◇, ◆), and 10 000 Hz (△, ▲) at zero applied field and $\chi'(T)$ (closed symbols) and $\chi''(T)$ (open symbols) for $Cr^{II}_{0.5}Cr^{III}[V^{II}(CN)_6]\cdot 0.1MeCN$ (**3**) (bottom) at 33 (○, ●), 100 (■, □), 1000 (◇, ◆), and 10 000 Hz (△, ▲) at zero applied field.

The best fits to the high-temperature region came from the reported temperature ranges, and the nature of this strange effect warrants a further discussion (vide infra). Overall, the change in the solvent significantly changes the magnitude of the maximum in $\chi T(T)$ and T_N of these similar compounds.

The frequency-dependent in-phase, $\chi'(T)$, and out-of-phase, $\chi''(T)$, components of the ac susceptibility can also be used to determine the ordering temperatures of **2** and **3**, and in a zero applied dc field, two drastically different responses dependent on the degree of solvation (z) are observed. In the 33-Hz data, the solvated **2** has a broad peak in the $\chi'(T)$ data that below 125 K has a maximum at 30 K, while in the $\chi''(T)$ data, a comparable broad peak is present below 110 K (maximum at 38 K) and has a shoulder at 17 K (Figure 3a). The presence of the broad peak and shoulder, which are present in all samples in differing amounts, suggests that two different magnetic components, each with different magnetic properties, are present in **2**. Desolvated **3** also exhibits a peak in the $\chi'(T)$ data (33-Hz data) below 125 K with a maximum at 23 K, but it is not as broad as that in **2**, while in the $\chi''(T)$ data, a very sharp peak occurs below 30 K with a maximum at 23 K (Figure 3b). From a rise in the $\chi''(T)$ data at the lowest frequency (33 Hz), the ordering temperatures of **2** and **3** were determined to be 110 and 25 K, respectively.[37] Note that these values are substantially different from the T_N values obtained above and are discussed below.

Compound **2** has no observable frequency dependence (ϕ[38] ≈ 0) for the higher-temperature ac peak, corresponding to a crystalline component with little to no disorder; however, there is a frequency dependence ($\phi = 0.07$) in the peak at 17 K (shoulder in the ac data of **2**). Similarly, the ac peak in **3** exhibits a small frequency dependence ($\phi = 0.02$), and both of the values of ϕ for the low-temperature peak for **2** as well as the only peak for **3** are consistent with a spin- or cluster-glass behavior.[38a] Spin-glass behavior has been reported for other Prussian blue magnets[39] and is indicative of a more disordered and/or amorphous material. The temperature at which the maximum in the $\chi'(T)$ data is frequency-dependent corresponds to the temperature at which the magnetic moments of these disordered materials become frozen (T_f).[38a] These data are consistent with the XRD patterns where **2** has both an amorphous and a fcc [a = 10.55(2) Å] crystalline component (Figure S5a in the Supporting Information), while **3** is structurally amorphous (Figure S5b in the Supporting Information) because of the lack of distinct diffraction peaks. Therefore, **3** is structurally amorphous, exhibiting a cluster-glass behavior resulting in a T_f of 25 K, and **2** is a mixture of a crystalline portion that is structurally ordered, leading to a ferrimagnetic phase with a higher T_c of 110 K and an amorphous portion (second magnetic phase) with a T_f similar to that of **3**. **3** could be considered as a pure material of the second magnetic phase in **2** (cluster-glass phase) and forms by the facile solvent loss of **2**.

These characteristic temperatures, T_c (110 K for **2**) and T_f (25 K for **3**), are substantially different from the T_N values (188 K for **2** and 153 K for **3**) obtained using Néel's hyperbola equation (vide supra). This deviation can be rationalized because at T_N nucleation of clusters in which long-range ferrimagnetic ordering is established within a sea of paramagnetic material begins to occur. These ferrimagnetic clusters are present in **2**, and much less so in **3**, and are localized in the crystalline portions of the material. Upon growth of these ferrimagnetic clusters, a rise in the $\chi T(T)$ data is expected and observed (Figure 2). In **2**, the clusters become sufficiently large and ferrimagnetic ordering is

(37) A variation in T_c from 100 to 125 K for **2** was observed and was dependent on the amount of solvent, z, in the compound. This is ascribed to **2**'s facile solvent loss at room temperature. Because the compound with a T_c of 110 K was the best characterized sample, we used it for comparisons. In contrast, samples of **3** were quite consistent in the values of T_c over several samples with a small range of 24 ± 1 K.

(38) (a) Mydosh, J. A. *Spin Glasses: An Experimental Introduction*; Taylor and Francis: London, 1993; p 67. (b) ϕ is a parameter indicative of the amount of spin disorder in a material known as spin-glass behavior: $\phi = \Delta T_{max}/[T_{max}(\Delta \log \omega)]$, where ΔT_{max} = difference between peak maximum of the temperatures at the high and low frequencies, T_{max} = peak maximum of the temperature at low frequency, and $\Delta \log \omega$ = difference in the logarithms of the high and low frequencies (ω).

(39) Buschmann, W. E.; Ensling, J.; Gütlich, P.; Miller, J. S. *Chem.—Eur. J.* **1999**, *5*, 3019. Sendek, M.; Csach, K.; Kavecansky, V.; Lukácová, M.; Marysko, M.; Mitróová, Z.; Zentko, A. *Phys. Status Solidi A* **2003**, *196*, 225.

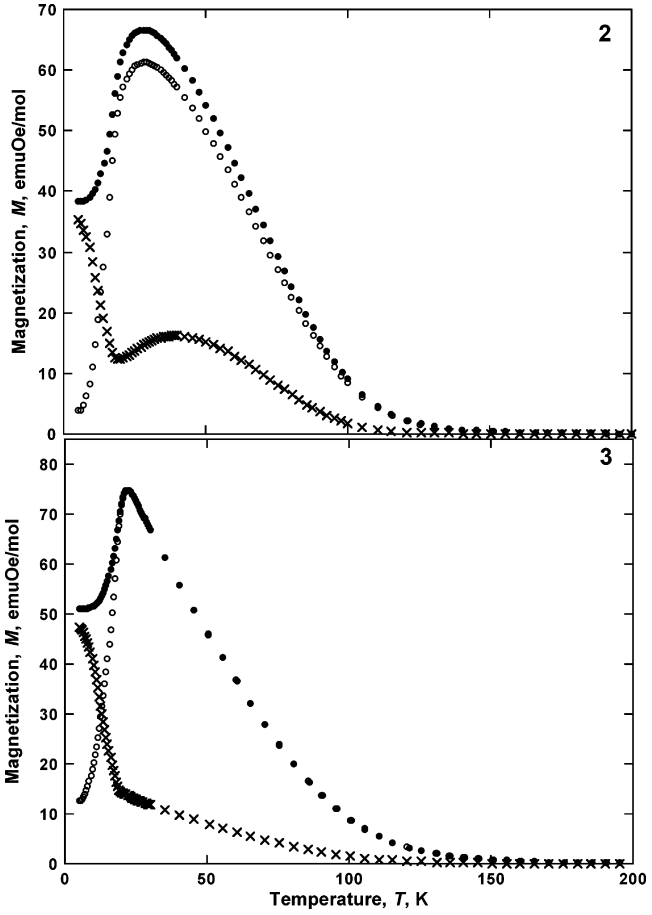

Figure 4. 5-Oe ZFC (●) and FC (○) $M(T)$ and $M_r(T)$ (×) data for **2** (top) and **3** (bottom).

established at a T_c of 110 K. In contrast, for **3**, with little to no crystalline portion, these ferrimagnetic clusters do not grow to the point where bulk ordering is observed; however, the moments generated within these clusters become frozen at a T_f of 25 K, resulting in the observed cluster-glass behavior. Zero-field-cooled/field-cooled (ZFC/FC) data support these characteristic temperatures in which $\chi_{FC}(T) \neq \chi_{ZFC}(T)$ and are termed the irreversibility or blocking temperature (T_b; Figure 4). In **2**, T_b is 105 K and attributed to a small irreversibility caused by the formation of spin domains after bulk ferrimagnetic order is established. In contrast, for **3** ($T_b = 21$ K), a large irreversibility is observed and is a consequence of the amorphous nature inherent with cluster-glass behavior.

Alternatively, the temperature at which the remnant magnetization, $M_r(T)$, goes to zero is also a determination of T_c. $M_r(T)$ values for **2** and **3** (Figure 4) are complicated. Nonetheless, both materials exhibit initial decreases in $M_r(T)$ as T is increased to 20 K. Above this temperature, differences occur, as **2** exhibits an increase in $M_r(T)$ that reaches a maximum at ~40 K while **3** changes slope and decreases more gradually. This increase of $M_r(T)$ for **2** and the change in slope for **3** are unusual and currently are under investigation. Both samples finally approach zero magnetization at ~120 K. This further suggests that both samples are mixtures of differing amounts of the ferrimagnetic and cluster-glass phases; however, only **3** has a small amount of the ferrimagnetic phase due to the absence of its peak in the $\chi''(T)$ data.

Field-dependent magnetization, $M(H)$, measurements show that **2** and **3** do not reach saturation below 90 kOe at 2 K and that their 90-kOe magnetization values are 2910 ± 470 emu Oe mol^{-1} for **2** and 1870 ± 435 emu Oe mol^{-1} for **3**.[40] These values are significantly lower than the expected 11 200 emu Oe mol^{-1} for high-spin Cr^{II} ($S = 2$), Cr^{III} ($S = {}^3/_2$), and V^{II} ($S = {}^3/_2$) calculated assuming that the magnetic interactions between adjacent metal centers are antiferromagnetic. The low high-field values of magnetization are attributed to the mixture of the ferrimagnetic (crystalline) and cluster-glass (amorphous) phases, which have significantly different magnetic properties. At 2 K, the spins of the ferrimagnetic phase ($T_c = 110$ K) are perfectly antiferromagnetically ordered, resulting in the expected saturation magnetization of 11 200 emu Oe mol^{-1}, and the shape of the curve should be consistent with ferrimagnetically ordered systems (s-shaped curve). In contrast, the spins of the cluster-glass phase ($T_f = 25$ K) are frozen randomly (*pseudo*paramagnetic) and do not perfectly align antiferromagnetically. This randomness of spins results in a more paramagnetic-like response in the $M(H)$ data, requiring significantly higher fields to saturate the magnetization. Therefore, the $M(H)$ data for **2** and **3** consist of a combination of both effects, and the observed response depends significantly upon the crystalline-to-amorphous ratio. From the $M(H)$ data for **2**, there is a rapid increase in the magnetization with increasing field up to 750 emu Oe mol^{-1} at 2500 Oe, and then it more gradually increases up to 90 kOe without saturation occurring. In contrast, **3** exhibits a paramagnetic-like response and does not reach 750 emu Oe mol^{-1} until 12 000 Oe in accordance with **3** having a larger amorphous fraction. However, because of the s-shaped curvature and hysteresis, it is clear that a portion of the crystalline fraction is still present. Determination of the amounts of these fractions in **2** and **3** is not trivial, and variations arise because of facile solvent loss at ambient conditions. Nevertheless, hysteresis curves are observed with coercive fields (H_{cr}) of 890 and 3900 Oe and remnant magnetizations of 500 and 400 emu Oe mol^{-1} for **2** and **3**, respectively (Figure 5). The large coercivity of **3** is consistent with it being more disordered than **2** because more magnetic energy is needed to flip the spins that are randomly frozen in a glassy disordered system than in a crystalline ordered system.

Conclusion

1a has been synthesized and enables the design of new Prussian blue structured magnetic materials. The reaction of $[V^{III}(CN)_6]^{3-}$ with $[Cr^{II}(NCMe)_6]^{2+}$ forms $Cr^{II}_{0.5}Cr^{III}[V^{II}(CN)_6]\cdot z$MeCN ($z = 0.1$ and 1.2). These new magnetic materials, although similar in composition, have significantly different magnetic behaviors, directly related to the degree

(40) The low magnetization values at 90 kOe and 2 K were observed for three samples of **3** and two samples of **2**. These variations are due to small changes in the solvent content, z.

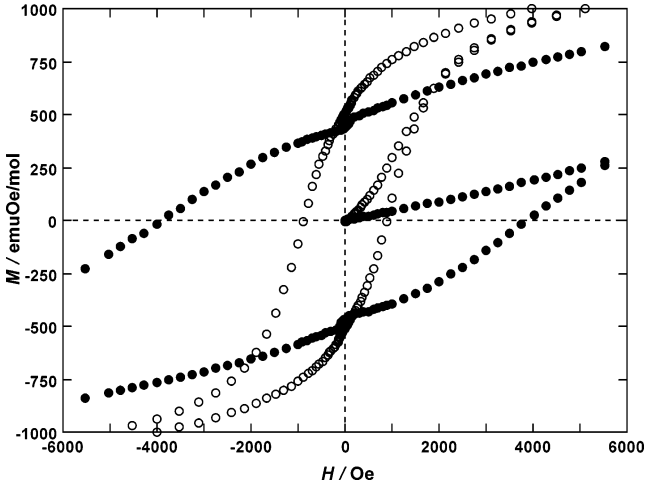

Figure 5. Magnetic hysteresis curves of **2** (○) and **3** (●) demonstrating the large change in H_{cr} of 3000 Oe upon desolvation.

of solvation (z). Both **2** and **3** are mixtures of two magnetic phases in differing amounts, with one being a bulk ferrimagnet (T_c = 110 K) and the other a cluster-glass phase (T_f = 25 K). The ferrimagnetic phase had no observable frequency dependence in the ac susceptibility and is consistent with the XRD data, which was indexed to a fcc structure [a = 10.55(2) Å], being more structurally ordered. In contrast, the cluster-glass phase has a small frequency dependence in the ac susceptibility (ϕ = 0.07 for **2**; ϕ = 0.02 for **3**) consistent with disorder that was also observed in XRD by the absence of sharp diffraction peaks. From this mixture of magnetic phases, **2** and **3** have complex magnetic responses [i.e., ac, ZFC/FC, $M_r(T)$, $\chi T(T)$, etc.]; nevertheless, both exhibit hysteretic effects with coercivities of 890 and 3900 Oe observed for **2** and **3**, respectively. Controlling the degree of solvation enables a substantial change in the overall magnetic properties of this new Prussian blue structured material [ferrimagnetic phase T_c = 110 K to the cluster-glass phase with T_f = 25 K (ΔT_c = 85 K) and ΔH_{cr} = 3000 Oe]. This modulation of T_c with the degree of solvation has been observed for several systems including a smaller 33 K change for $K_{0.2}Mn_{1.4}[Cr(CN)_6]\cdot 6H_2O$.[12] A further study into the degree of solvation and its effects on both structural and magnetic properties, as well as the synthesis of similar compounds without mixed valence character, is currently under investigation.

Acknowledgment. The authors gratefully acknowledge the helpful discussion with K. I. Pokhodnya as well as the continued partial support from the U.S. Department of Energy, Basic Energy Sciences (Grant DE FG 03-93ER45504), and the AFOSR (Grant F49620-03-1-0175).

Note Added after ASAP Publication. This article was released ASAP on October 3, 2006, with minor errors throughout the paper. The correct version was posted on October 16, 2006, with the addition of ref 24b and changes in the discussion of high T_N values for **2** and **3**.

Supporting Information Available: X-ray crystallographic data in CIF format for **1** and Figures S1−S6. This material is available free of charge via the Internet at http://pubs.acs.org.

IC0608896